LETTER TO THE EDITOR

Probing the Structural Changes in the Phase Transitions of a Bi₂MoO₆ Catalyst: The Nature of the Intermediate-Temperature Phase

Gopinathan Sankar, Mark A. Roberts, and John Meurig Thomas[1]

Davy Faraday Research Laboratory, The Royal Institution of Great Britain, 21 Albemarle Street, London W1X 4BS, United Kingdom

and

G. U. Kulkarni, N. Rangavittal, and C. N. R. Rao[1]

Solid State and Structural Chemistry Unit, Indian Institute of Science, Bangalore—560 012, India and Department of Chemistry, University of Wales, Cardiff CF1 3TB, United Kingdom

The nature of the phase transitions of Bi_2MoO_6 has been investigated by the combined use of X-ray diffraction and X-ray absorption spectroscopy. The distorted MoO_6 octahedra in the low-temperature form are shown to undergo further distortion in the intermediate-temperature form before transforming to MoO_4 tetrahedra in the high-temperature phase. © 1995 Academic Press, Inc.

Bismuth molybdates are widely used for the catalytic conversion of olefins to unsaturated aldehydes. For example, a typical selectivity of ca. 95% has been achieved using this catalyst for the oxidation of propylene to acrolein. Recent reviews summarize the catalytic properties of multicomponent bismuth molybdate catalysts (1, 2); in particular, it was shown that the $Bi_2O_3 \cdot nMoO_3$ phases with $n = 3$ (α form), $n = 2$ (β form), and $n = 1$ (γ form) are responsible for the catalytic activity. Although the phase diagram of bismuth molybdate has been investigated in detail (3), only some of the structures of these mixed metal oxide systems are fully established. In order to understand the structure and its relationship to the observed catalytic properties, several bismuth molybdate phases have been investigated using X-ray diffraction (4–10), high-resolution electron microscopy (3–6, 11, 12), neutron diffraction (13, 14), and vibrational spectroscopy (15). An earlier X-ray adsorption spectroscopy study investigated these three forms, probing both BiL_3- and MoK-edges (16). Of these

the γ- form (which is the naturally occurring mineral koechlinite) exhibits interesting phase transformations at elevated temperatures (11). The phase transformation of Bi_2MoO_6 from the γ to the γ' form takes place above 600°C through the formation of the intermediate γ'' phase. The crystal structure of the room-temperature γ phase has been described adequately in the literature (3–15) and the structure of the high-temperature γ' form has been discussed recently (12, 14). The low-temperature phase consists of layers of corner-shared MoO_6 octahedra separated by Bi_2O_2 layers whereas in the high-temperature γ' form molybdenum is in tetrahedral coordination with oxygen.

Here we focus our attention on the study of the transformation of Bi_2MoO_6 from the γ form to the γ' form under dynamic conditions. For this purpose, we have made use of a combination of two powerful structural techniques, namely, X-ray absorption spectroscopy (XAS) and X-ray diffraction (XRD), to probe both short-range (around molybdenum) and long-range structures, respectively. We have employed the recently developed combined XAS/XRD technique with synchrotron radiation (17–21). Preedge features in XAS have been used extensively in the literature to characterize the local environment around metal ions in many oxidic materials including catalytic systems (16, 23, 24). The use of intense synchrotron radiation, a position-sensitive INEL detector (for XRD measurement), and QuEXAFS (acronym for quick EXAFS) permits time resolution for dynamic studies during either an isothermal process or a ramping with appropriate tempera-

---

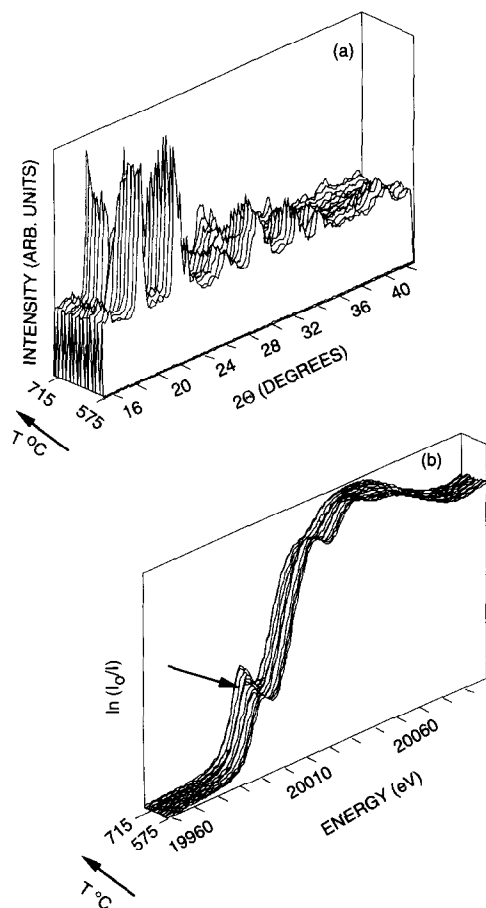[1] To whom correspondence should be addressed.

FIG. 1. Combined XRD/XAS patterns of Bi_2MoO_6 data collected during the heat treatment (in air) between 575 and 715°C. XRD data (a) were collected below the MoK-edge at a wavelength of 0.62717 Å and the MoK-edge XAS (b) data were collected ca. 150 eV below the edge and ca. 700 eV above the edge. A narrow region (in both XRD and XAS) of the data is presented here to bring out clearly the various features in the spectra. The change in the preedge feature during the transformation is indicated with an arrow in (b).

ture steps (17, 19). With the aid of this combined technique, as well as with the data recorded using a conventional high-resolution laboratory X-ray powder diffractometer, we discuss the phase transformations of Bi_2MoO_6, in particular the nature of the intermediate-temperature γ'' phase and its relation to the γ and γ' phases.

The γ form of Bi_2MoO_6 was prepared by a coprecipitation method, in which stoichiometric amounts of $(NH_4)_6Mo_7O_{24} \cdot 4H_2O$ (in NH_4OH) and $Bi(NO_3)_3 \cdot 5H_2O$ (in dilute HNO_3) were simultaneously added to a beaker with rapid stirring. The pH was adjusted to the range from 6 to 7 using ammonia. The resulting slurry was heated to boiling, until it was dry. The nitrate was then sublimed by heating at 425°C for 3 hr and the remaining mixture was calcined at 530°C for 20 hr. High-resolution XRD measurements were carried out over the range 300–650°C using a

STOE high-resolution powder diffractometer employing CuK_α radiation.

Combined XRD/XAS measurements were carried out on station 9.3 at Daresbury Synhcrotron Radiation Source, using the experimental setup described elsewhere (17, 19). A self-supporting wafer of the γ-Bi_2MoO_6 sample was loaded into a specially designed high-temperature furnace that permits the measurement of diffraction data covering a large 2Θ angle (9° to 70°) and XAS by both transmission
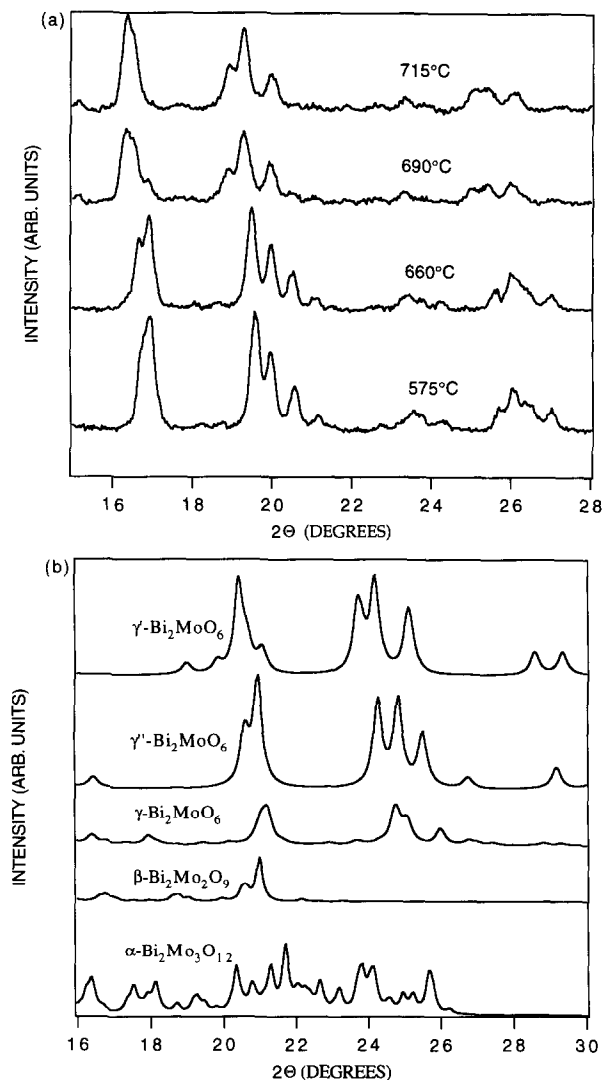

FIG. 2. (a) XRD data collected at 575, 660, 675, and 715°C. A narrow range of data is plotted to highlight the changes in the reflections corresponding to different phases. (b) Simulated XRD data of $Bi_2O_3 \cdot nMoO_3$ with $n = 3$ (α phase), $n = 2$ (β phase), and $n = 3$ (γ phase, γ'' phase, and γ' phase) are shown here. For the simulation the JCPDS database (27–31) was used with IDF software (Siemens). The FWHM and 2Θ step size used for the simulation are identical to those of the experimental data collected using an INEL position-sensitive detector (PSD) present in the XRD/XAS setup. The PSD was calibrated using a NBS silicon standard.
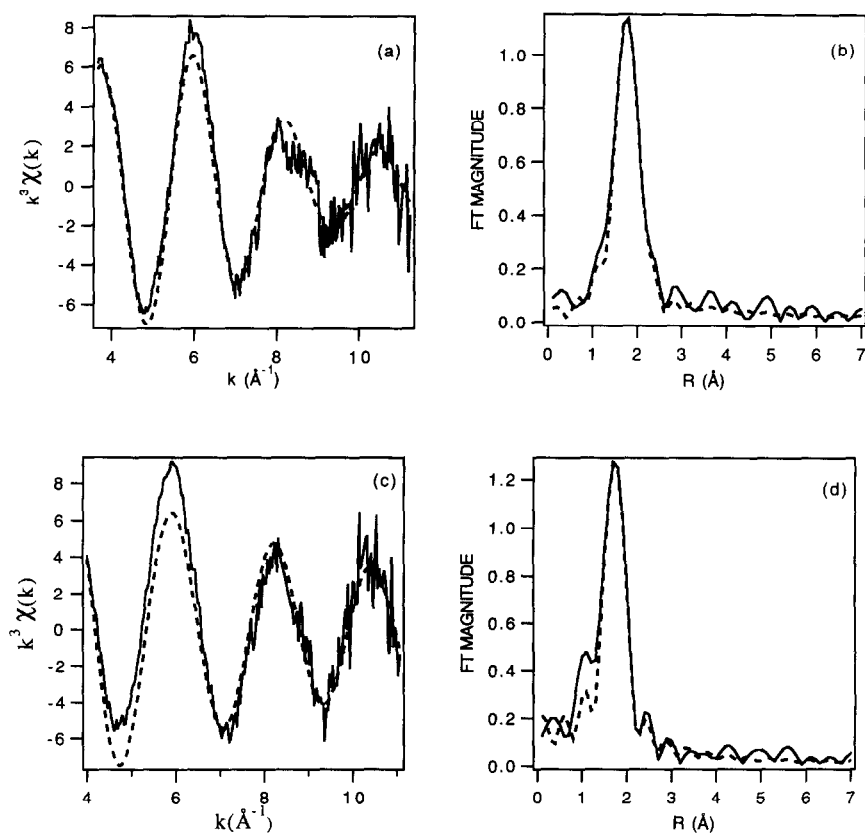
FIG. 3. (a) Best fit to the MoK-edge EXAFS data and (b) the respective Fourier transforms of Bi_2MoO_6 recorded at 570°C. The corresponding curves at 715°C are given in (c) and (d), respectively. The solid line shows the experimental data and the dashed line represents the calculated data using a nonlinear least-squares procedure.

and fluorescence modes (21, 25, 26). In this study, MoK-edge XAS data were collected using transmission mode and the XRD data were measured below the MoK-edge using a wavelength of 0.62717 Å. XAS and XRD data were collected for 263 and 120 sec, respectively, so that the total cycle time is 420 sec, including the deadtime. Initially, the temperature was raised from room temperature to 575°C at the rate of 5°C/min, during which data collection was not performed, and from 575°C to 715°C at the rate 2°C/min, during which the XRD and XAS data were collected. Finally, the sample was retained at 715°C for 15 min. XAS data were analyzed using a suite of programs, namely EX-CALIB (for converting the data collected to absorption coefficient vs energy), EXBROOK (for pre- and postedge background subtraction), and EXCURV92 (for nonlinear least squares curve-fitting analysis).

The XRD and XAS patterns of Bi_2MoO_6 recorded during the heating process between 575 and 715°C are shown in Figs. 1a and 1b, respectively. Changes in the XRD pattern and the X-ray absorption near-edge structure (XANES) are distinctly visible in these figures. In interpreting the XANES results, we have employed $Na_2MoO_4 \cdot 4H_2O$ containing MoO_4 tetrahedra and MoO_3 con-

taining distorted MoO_6 octahedra as model compounds (24). The XANES in Fig. 1 shows a clear change in the edge feature accompanying the γ-γ' transformation. The γ form, which contains Mo^{6+} in distorted octahedra shows a weak shoulder (preedge feature) and a distinct peak in the main absorption, both of which are in accordance with the known structure (16). As the γ form is heated, the XANES features undergo dramatic changes around 670°C. The increase in the preedge intensity and the decrease in the intensity of the shoulder on the top of the edge signify the formation of tetrahedral coordination around molybdenum, consistent with the known XANES features of tetrahedral and octahedral environments around molybdenum in the model compounds. Although the preedge intensity of the γ'-Bi_2MoO_6 phase is intense, it is not as well defined as that in $Na_2MoO_4 \cdot 4H_2O$, possibly due to a distorted four-coordinated Mo–O environment (14).

In order to establish the nature of the phases formed in the transformation of γ-Bi_2MoO_6 and to exclude the possibility of the formation of the β phase, consisting of Mo^{6+} in tetrahedra coordination (16), we have carefully examined the XRD patterns of the different phases. The changes that occur in the XRD patterns (measured using
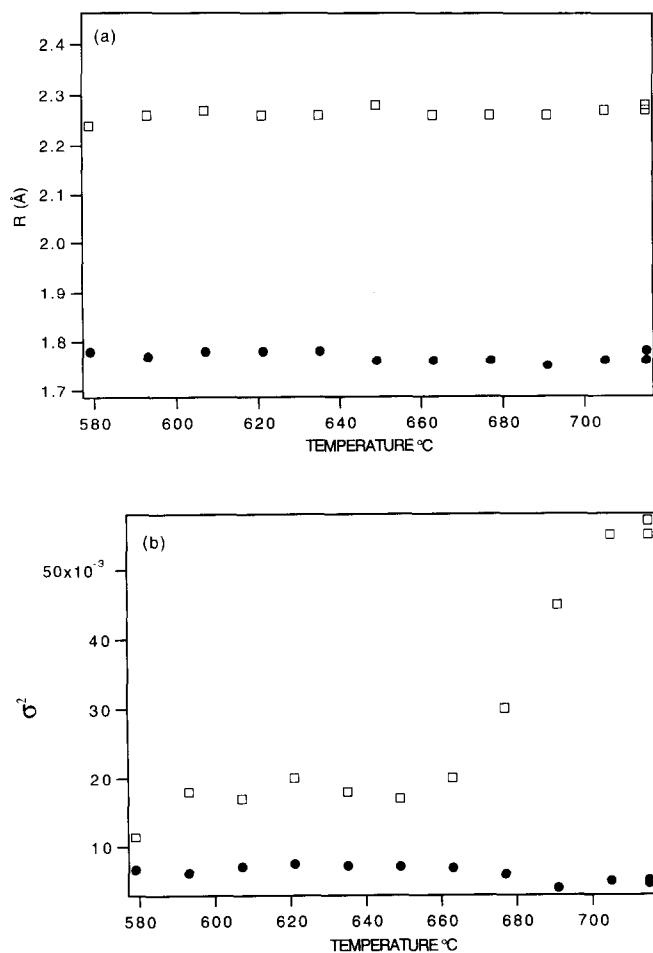
FIG. 4. Temperature variation of the (a) Mo–O distances and (b) the Debye–Waller factor (2). The filled circles and open squares show the data corresponding to the short and long Mo–O distances, respectively.

XRD patterns in Fig. 2 clearly show that the temperature-induced changes in the pattern of Bi_2MoO_6 are due to the phase changes.

For the analysis of the EXAFS data, the crystallographic information concerning the Mo–O distances were taken into consideration. Accordingly, the four Mo–O distances in the range 1.75 to 1.93 Å of the γ phase were taken as a single shell (compensated by static disorder of the Debye–Waller factor, σ^2) to avoid any correlation effects. The two long distances at ca. 2.20 Å were considered as a separate shell. In Fig. 3, we have shown the fits to the experimental EXAFS obtained by us along with the Fourier transforms of the data collected at 575 and 715°C, representative of the γ and γ' phases, respectively. In the analysis, the coordination number was fixed for the two shells, namely 4 and 2, since the coordination number is highly correlated with the Debye–Waller factor. The Mo–O distances and the Debye–Waller factor of the two average Mo–O interatomic distances starting with the γ phase are plotted against temperature in Fig. 4. The Debye–Waller factor for the first shell initially increases and starts to decrease close to the transformation temperature. The σ^2 of the longer Mo–O distance increases throughout and more rapidly above the transformation; this behavior suggests that there is more ordering in the short Mo–O distance and that the presence of a long Mo–O distance is suppressed. This is consistent with our XANES results as well as other studies (14) showing that the high-temperature γ' form consists of four coordinated Mo^{6+} with an average Mo–O distance of 1.76 Å, compared to the distorted octahedral coordination of the low-temperature γ phase (7). In contrast to the high-temperature γ' form, the intermediate-temperature γ'' form, occurring around 610°C, does not show the presence of MoO_4 tetrahedra.

the combined XRD/XAS experiment) during heating are shown in Fig. 2a, where we have plotted the XRD patterns recorded at 575°C (well below the transformation), 660°C (just below the $\gamma-\gamma'$ transformation, i.e., before the change in the edge structure), 690°C (just after the transformation, i.e., immediately after the change in the edge structure), and 715°C. We have simulated the XRD patterns of the α and β phases of $Bi_2O_3 \cdot nMoO_3$ with $n = 3$ and 2 (27, 28) as well as of the γ, γ'', and γ' phases (29–31), using the data provided in the JCPDS database. In doing so, the FWHM and the interval between data points of the simulated data were kept comparable to those of experimental data by calibrating the combined XAS/XRD setup using a NBS silicon standard. The simulated XRD patterns are shown in Fig. 2b. Note that the wavelength used in the experiment is different (well below the MoK-edge to avoid fluorescence effects, $\lambda = 0.62717$ Å) from that of the simulated data. For the simulated data, the standard MoK_α wavelength ($\lambda = 0.7093$ Å) was used. The
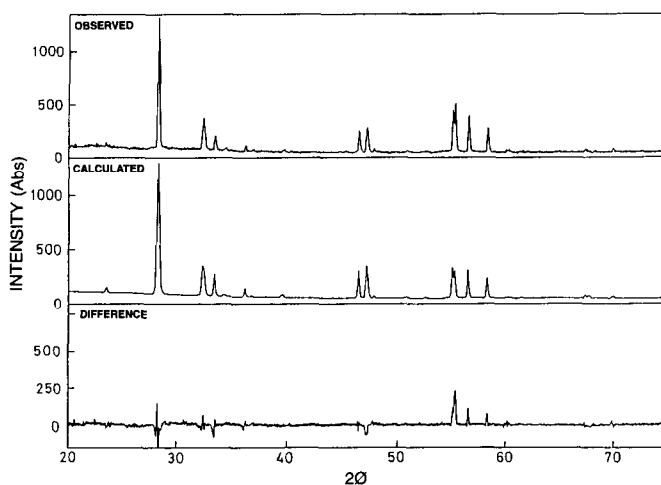

FIG. 5. Observed, calculated, and difference X-ray powder diffraction profiles of the γ'' phase (610°C). The data were collected using $CuK\alpha$ radiation.
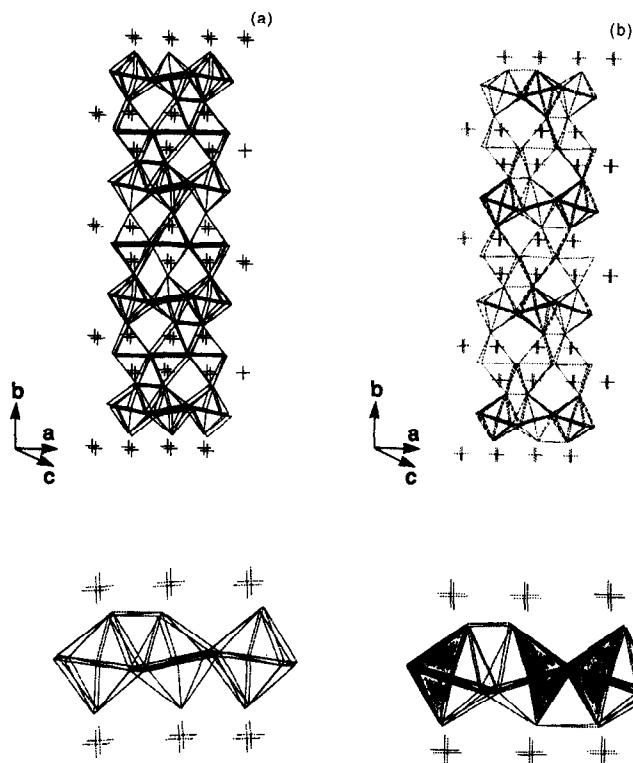
FIG. 6. Structural projections of (a) γ and (b) γ'' phases of Bi_2MoO_6.

The XANES and EXAFS data collected during the formation of the intermediate γ'' phase (identified using XRD) establish that the γ'' phase still consists of a distorted octahedral environment. In what follows, we elaborate on the structure of the γ'' phase.

Since the γ'' form involves MoO_4 tetrahedra in contrast to MoO_6 octahedra in the γ phase, it was of interest to obtain the structure of the intermediate γ'' phase. We have carried out a Rietveld refinement analysis of the high-resolution X-ray profiles of Bi_2MoO_6 recorded at 610°C. Prior to this analysis, it was ascertained that the profile refinement of the model of the γ form gave the known structure. The space group of the γ'' phase was identical to that of the γ phase ($Pca21$) with unit cell dimensions of $a = 5.5383(6)$, $b = 16.1610(5)$, and $c = 5.5649(6)$ Å (this must be compared with unit cell dimensions of the form $a = 5.5012(6)$, $b = 16.2584(5)$, and $c = 5.5218(6)$ Å). There is an expansion of the unit cell volume by about 4 Å³. We could get a reasonable fit to the experimental profile, by employing the structure of the γ form as the starting model, as shown in Fig. 5. In Table 1, we compare the Mo–O distances in the γ and γ'' phases obtained in the present study. We note that the increase in the a and c parameters results in an increase in the in-plane Mo–O distance (1.76 and 1.84 Å). The two apical distances (1.85 and 1.92 Å), on the other hand, undergo contraction. The two larger

in-plane Mo–O distances in the room-temperature form become even longer, leading to large distortions in the MoO_6 octahedra. These distances show how Mo is bonded to the two oxygens present at a distance of more than 2.21 Å. It is as though the octahedra in the γ'' phase are at the verge of becoming tetrahedra. Structural projections of the γ and γ'' phases are illustrated in Fig. 6 to show how the octahedra in the γ'' phase are more distorted than those in the γ form.

The present study establishes how the transformation of the MoO_6 octahedra in the room-temperature phase to the MoO_4 tetrahedra in the high-temperature phase occurs. This involves a progressive increase in octahedral distortion with an increase in temperature up to the γ''–γ' transformation.

ACKNOWLEDGMENTS

REFERENCES

1. Y. Moro-Oka and W. Ueda, Adv. Catal. 40, 233 (1994).
2. R. K. Grasseli and J. D. Burrington, Adv. Catal. 30, 133 (1981).
3. D. J. Buttrey, D. A. Jefferson, and J. M. Thomas, Philos. Mag. A 53, 897 (1986).
4. A. F. Van den Elzen and G. D. Rieck, Mater. Res. Bull. 10, 1163 (1975).
5. D. J. Buttrey, D. A. Jefferson, and J. M. Thomas, Mater. Res. Bull. 21, 739 (1986).
6. Z. Wuzong, D. A. Jefferson, M. Alario-Franco, and J. M. Thomas, J. Phys. Chem. 91, 512 (1987).
7. N. Rangavittal, Ph.D. Thesis, Indian Institute of Science, Bangalore, 1995.
8. A. F. Van den Elzen and G. D. Rieck, Acta Crystallogr. Sect. B 29, 2433 (1973).
9. A. F. Van den Elzen and G. D. Rieck, Acta Crystallogr. Sect. B 29, 2436 (1973).
10. H. Y. Chen and A. W. Sleight, J. Solid State Chem. 63, 70 (1986).

11. A. Watanabe, S. Horiuchi, and H. Kodama, *J. Solid State Chem.* **67,** 333 (1987).
12. P. L. Gai, *J. Solid State Chem.* **49,** 25 (1983).
13. F. Theobald, A. Laarif, and A. W. Hewat, *Mater. Res. Bull.* **20,** 653 (1985).
14. D. J. Buttrey, T. Vogt, U. Wildgruber, and W. R. Robinson, *J. Solid State Chem.* **111,** 118 (1994).
15. F. D. Hardcastle and I. E. Wachs, *J. Phys. Chem.* **95,** 10,763 (1991).
16. M. R. Antonio, R. G. Teller, D. R. Sandstrom, M. Mehicic, and J. F. Brazdil, *J. Phys. Chem.* **92,** 2939 (1988).
17. J. M. Thomas and G. N. Greaves, *Catal. Lett.* **20,** 337 (1993).
18. B. S. Clausen, K. Graback, G. Steffensen, P. L. Hansen, and H. Topsoe, *Catal. Lett.* **20,** 23 (1993).
19. G. Sankar, J. M. Thomas, P. A. Wright, S. Natarajan, A. J. Dent, B. R. Dobson, C. A. Ramsdale, G. N. Greaves, and R. H. Jones, *J. Phys. Chem.* **97,** 9550 (1993).
20. J. M. Thomas and G. N. Greaves, *Science* **265,** 1675 (1994).
21. P. A. Barrett, G. Sankar, C. R. A. Catlow, and J. M. Thomas, *J. Phys. Chem. Solids,* to appear.
22. M. A. Roberts, G. Sankar, C. R. A. Catlow, and J. M. Thomas, presented at "Synchrotron Radiation in Materials Science," Chester, United Kingdom, 1994.
23. G. Sankar, F. Rey, J. M. Thomas, G. N. Greaves, A. Corma, A. J. Dent, and B. R. Dobson, *J. Chem. Soc. Chem. Commun.,* 2279 (1994).
24. M. de Boer, A. J. van Dillen, D. C. Koningsberger, J. W. Geus, M. A. Vuurman, and I. E. Wachs, *Catal. Lett.* **11,** 227 (1991).
25. A. J. Dent, M. Oversluizen, G. N. Greaves, M. A. Roberts, G. Sankar, C. R. A. Catlow, and J. M. Thomas, *Physica B* **208/209,** 253 (1995).
26. J. M. Thomas, G. N. Greaves, G. Sankar, P. A. Wright, J. Chen, A. J. Dent, and L. Marchese, *Angew. Chem. Int. Ed. Engl.* **33,** 1871 (1994).
27. JCPDS Card No. 21-103.
28. JCPDS Card No. 33-209.
29. JCPDS Card No. 21-102.
30. JCPDS Card No. 22-113.
31. JCPDS Card No. 33-208.